The Indonesian Journal of Computer Science
www.ijcs.net
Volume 14, Issue 1, February 2025
https://doi.org/10.33022/ijcs.v14i1.4728

Comparative Analysis of Battery SOC Depletion and Driving Range of PMSM-driven Electric Vehicle (EV) using Sinusoidal PWM (SPWM) and Space Vector PWM (SVPWM) Control

Khin Maung San[1], Wunna Swe[2]
khinmaungsanssan007@gmail.com[1], swethunay@gmail.com[2]
Department of Electrical Power Engineering, Mandalay Technological University

Article Information

Received : 21 Feb 2025
Revised : 24 Feb 2025
Accepted : 26 Feb 2025

Keywords

Electric vehicle, decoupling control, sinusoidal pulse width modulation, space vector pulse width modulation, permanent magnet synchronous motor.

Abstract

Conventional vehicles utilize fossil fuels to provide a good performance and long range leading to exhaust gas emissions causing environmental pollution & low fuel economy. Electric vehicles are called future vehicles in the place of internal combustion engines because they work with pollution and are more efficient. In the impending future, the automotive industry is marching towards cleaner energy. This paper presents the comparative analysis of battery SOC and driving range of an electric vehicle (EV) with a decoupling control method using SPWM and SVPWM. Simulation tests have been carried out on an 80 kW Nissan Leaf EV that consists of a permanent magnet synchronous motor and a three-level inverter. The analysis is focused on MATLAB simulations, based on speed regulation, torque response, usage battery SOC, and travel range. For these closed-loop feedback control methods, the reference speed is obtained by driving an internal combustion engine (ICE) car in the mountain region of Southen Shan State, Myanmar for 60 sec.

A. Introduction

In recent years, the usage of EVs has increased due to the positive impacts such as there is no dependency on the depleting reserves of conventional fuels and they have environmentally friendly emissions when compared with the air pollution of ICE cars. The performance of electric vehicles has reached a higher level due to the recent improvements in electrical sources such as supercapacitors (SCs), fuel cells (FCs), and the advancements within conventional battery systems [1].

The electric motors of EVs get power from batteries, unlike an internal combustion engine that uses fossil fuel. The battery is charged with a plug-in charging unit such as an on-board charger and an off-board charger when the vehicle is not in use [2]. In addition, they enable charging the battery using renewable energy sources. EVs have some weaknesses, although they seem to be excellent in transportation. The main energy storage system, the battery, is still overpriced, and the trade-off between the vehicle range and the time of the charging process is long, and the cost for these units is expensive [6].

The electric machines supply torque and power to the drivetrain for the traction of EVs. Motor control is needed in many applications for the automotive environment that needs special requirements, e.g., higher reliability, working with varying conditions and working at low voltage levels, providing higher torque at high speeds with smaller size and higher efficiency. Nowadays, three-phase PMSMs are used in steering systems because of their compact design, high power density, excellent torque-to-weight ratio, smooth speed profile over the entire torque range, and high efficiency [2].An electric power-assisted steering system has overcurrent problems that occur during torque reversing at high-speed operations. Many overcurrents appear at the transient states during these conditions, and controllers don't have a fast response to compensate for internal changes in the PMSM. To solve these overcurrent problems, controllers are improved using the decoupling technique. The main purpose of the decoupling technique in many control systems is to improve the reliability of many applications without losing the torque output or decreasing system dynamic performances [8].

This study focuses on decoupling control with sinusoidal pulse width modulation (SPWM) technique and space vector pulse width modulation (SVPWM) technique schemes to regulate the speed and torque of an electric vehicle. The analysis mainly focused on the modeling of EV and control mechanisms. The voltage source converter uses PWM to control these converters. The switching devices are power semiconductors that can operate at high frequencies. There are several techniques to control semiconductor converters, and they have advantages and disadvantages. The SPWM is a mature technology. By comparing the carrier signal with the reference control signals, the SPWM is obtained. SVPWM is different from SPWM and they are better than SPWM. The realization of SVPWM is the proper selection of the inverter switching vectors, calculation of the appropriate switching devices, and space vector transformation[3].

B. Dynamic Vehicle Model

When the vehicle moves on the sloping road, the torque requirement in the longitudinal motion changes due to the varying driving conditions. The cruise control system keeps the vehicle's speed at the desired speed. In the vehicle moving process, the rolling resistance, the equivalent aerodynamic drag resistance, and the slope resistance affect the vehicle's performance, as shown in Figure 1. In real driving conditions, the vehicle's total mass is affected by the passenger number and the pitch angle that changes by the real-time road condition [7].

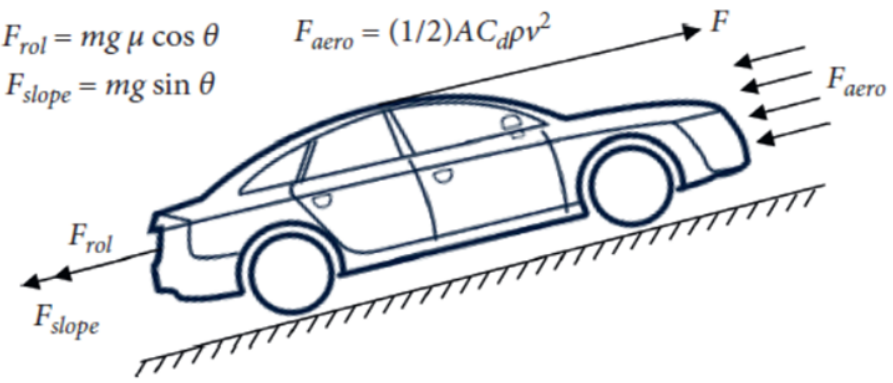

Figure 1. Vehicle Longitudinal Dynamics

The longitudinal dynamics model can be expressed as;

$$F = F_{rol} + F_{aero} + F_{slope} \quad (1)$$

Rolling resistance force is

$$F_{rol} = mg\mu\cos\theta \quad (2)$$

Slope resistance force is

$$F_{slope} = mg\sin\theta \quad (3)$$

The aerodynamic drag resistance force is

$$F_{aero} = \frac{1}{2} AC_d\rho v^2 \quad (4)$$

The resultant torque T in the longitudinal motion is

$$T = Fr \quad (5)$$

In Equations (2) & (3), the rolling resistance force and slope resistance forces vary depending on the vehicle pitch angle. According to Equation (5), the load torque varies on the slop road. As the load torque changes, traction motor torque needs to change. The relation between the load torque and the motor's torque can be represented by the Equation (6);

$$T_m = \frac{T}{i_g \eta_g} \quad (6)$$

Where; F is the resultant driving force and breaking force, m is the vehicle's total mass, g is acceleration due to gravity, μ is rolling resistance coefficient, θ is vehicle's pitch angle, A is frontal area of the vehicle, C_d is aerodynamic drag coefficient, ρ is air density, v = vehicle's speed, r is wheel's radius, T is load torque, T_m is motor torque, i_g is gear ratio and η_g is efficiency of mechanical system [5].

C. PMSM Mathematical Model and Decoupling Control

The d-q coordinates mathematical model is normally used to understand the decoupling of the mathematical model of PMSM, which is convenient for analyzing the steady-state and dynamic performances of PMSM. It is often necessary to ignore some parameters of the motor when building the mathematical model of PMSM, on the building of the mathematical model to simplify the analysis has little influence, and generally the following assumptions

(1) The motor core saturation is neglected;

(2) Hysteresis and eddy current losses of the motor are excluded;

(3) The current inside the motor is the symmetrical three-phase sine wave current.

With these conditions, the mathematical model of PMSM on the two-phase rotating coordinate system (d-q) is

$$V_d = R_s i_d + \frac{d\psi_d}{dt} - \omega_r \psi_q \quad (1)$$

$$V_q = R_s i_q + \frac{d\psi_q}{dt} + \omega_r \psi_d \quad (2)$$

$$\psi_{d=} \psi_f + L_d i_d \quad (3)$$

$$\psi_{q=} L_q i_q \quad (4)$$

$$T_e = \frac{3}{2} p[\psi_f i_q + (L_d - L_d) i_d i_q)] \quad (5)$$

Where; Vd, Vq, id, iq, Ld, Lq, ψd, and ψq are the quadrature axis, direct axis stator voltages, currents, inductances, and flux linkages. Rs is the stator resistance, ψf is the permanent flux linkage, ωr is the rotor electric angular velocity, p is the pole pairs, and Te is the electromagnetic torque.

Substituting the stator flux linkage Equations (3) and (4) into the stator voltage Equations (1) and (2).

$$V_d = R_s i_d + L_d \frac{di_d}{dt} - \omega_r L_q i_q \quad (6)$$

$$V_q = R_s i_q + L_q \frac{di_q}{dt} - \omega_r (L_d i_d + \psi_f) \quad (7)$$

As can be seen from Equations (6) and (7), the stator inductance parameter causes crosscoupling in the d-q axis, and the larger the ωr is the stronger the coupling effect, and its influence is greater in the variable speed and high speed regions. The structure of the PMSM decoupling control electric vehicle system is shown in Figure 2.

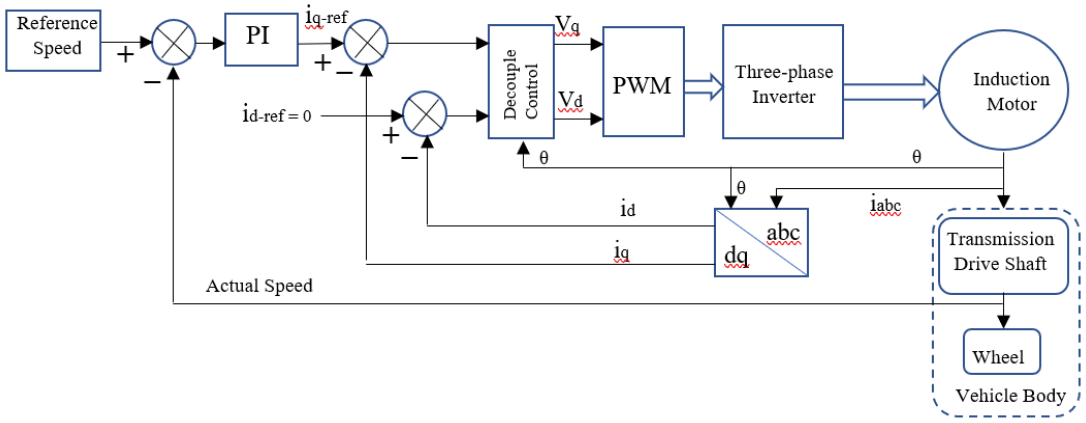

Figure 2. Structure of the PMSM Vector Control System.

The system has a double closed-loop control structure with an internal current loop and an external speed loop. The actual vehicle speed is compared with the reference speed to get the deviation number. This deviation signal is passed through the speed PI controller to obtain the quadrature axis current iq-ref of the stator current. The stator quadrature and direct axes currents of motor id, iq are feedbacked. The deviation signals obtained by comparing id-ref, iq-ref with id, iq are passed through the PI controllers to obtain the voltage signals, Vd, Vq in the d-q coordinate system [9].

From Equations (6) and (7), when a normal PI controller is used, it can be known that in the state equation, there is a coupling term. Part of the output voltages of the normal PI controller use the counter-electromotive force to offset. Part of this is used in controlling cross-direct axis current, this can reduce the regulation accuracy and increase the regulation time. Therefore, compensating coupling terms in Equations (8) and (9) in the normal current regulate the dynamic performances of the control method can be developed.

$$V_d^{'}=V_d+\omega_r L_q i_q \tag{8}$$

$$V_q^{'}=V_q-\omega_r L_d i_d-\omega_r \psi_f \tag{9}$$

Substituting Equations (8) and (9) in Equations (6) and (7).

$$V_d^{'}=R_s i_d+L_d \frac{di_d}{dt} \tag{10}$$

$$V_q^{'}=R_s i_q-L_q \frac{di_q}{dt} \tag{11}$$

According to the above equation, in the voltage equation, there is no coupling between them after compensation. Figure 3 shows the voltage feed-forward decoupled compensated current regulator design structure.

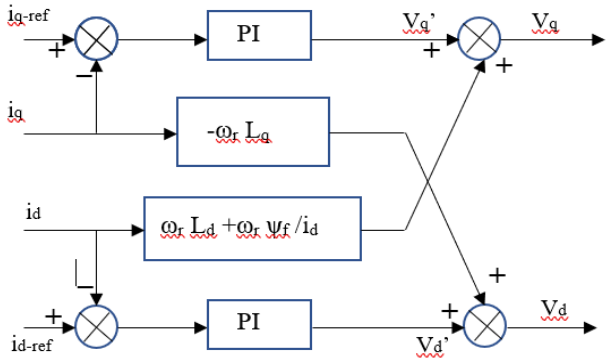

Figure 3. Decouple PI Feed-forward Structure

The voltage signals in the two-phase stationary coordinate system Vd, Vq are fed into the PWM algorithm to generate control pulses, which are used to control the switching state of the three-phase inverter and thus the three-phase symmetric winding of the stator obtains the actual current. In this method, the reference value of the stator current torque component is generated from the outer speed loop, and the actual control signal is obtained from the inner current loop, thus a complete speed-current double closed-loop control system is forming [9].

Sinusoidal Pulse Width Modulation (SPWM)

One of the useful switching methods in power-switching converters is sinusoidal pulse width modulation (SPWM). SPWM technique generates firing pulses to switch semiconductor devices; and determines the frequency and nature of the converter output AC voltage of the converter. The output voltage of the converter is controlled by adjusting the widths of the pulses. Figure 4 shows the gating signals generated from the intersection of sinusoidal modulating wave and high-frequency triangular wave [4].

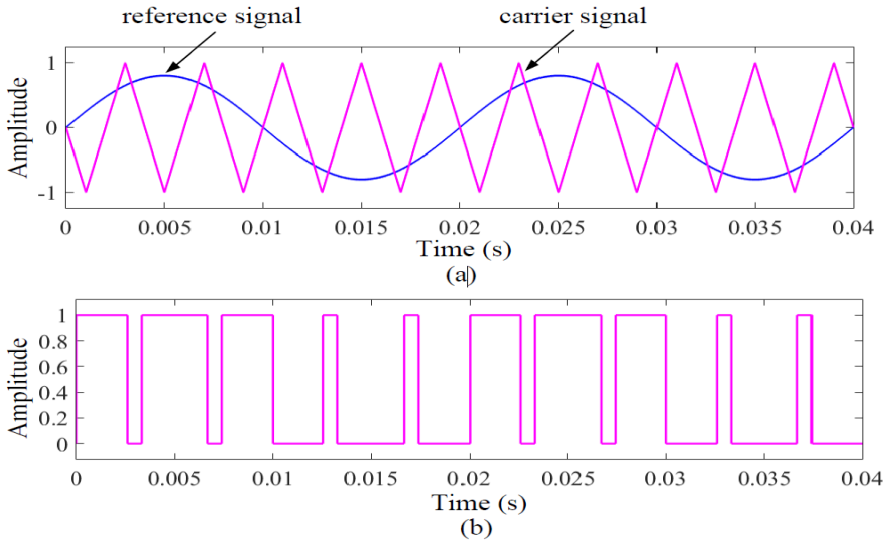

Figure 4. Sinusoidal PWM: (a) Reference and Carrier Signal Comparison (b) Gate Pulse Signals

The sinusoidal PWM technique can be used to control the magnitude and frequency of output voltages. The witching signals of the converter are obtained,

by comparing the sinusoidal modulating wave with the high switching frequency carrier wave (triangle wave). The carrier frequency is several times the reference frequency. When the reference signal is higher than the triangular signal, the PWM output signal is high (1). Otherwise, it is low (0). The output voltage and frequency depend on the magnitude and frequency of the sinusoidal wave. The output voltage is proportional to the magnitude of the sinusoidal wave, and the output frequency is equal to the sine wave frequency [4].

Space Vector Pulse Width Modulation (SVPWM)

Space vector pulse width modulation (SVPWM) is a useful technique, and this is used to control the switches of a three-phase inverter to produce a modulated voltage that drives a motor. SVPWM uses a DC voltage to emulate a three-phase sinusoidal waveform with adjustable frequency and amplitude. The goal is to produce a "mean vector" that matches the desired voltage vector. SVPWM is commonly used to control permanent magnet synchronous motors (PMSM) and induction motors.

SVPWM operates in the α-β frame rather than the ABC frame. The circuit configuration of a two-level three-phase inverter is shown in Figure 5. In the α-β frame, a space vector represents each switching condition of the inverter. Then, not to short-circuit the DC bus, the lower and upper switches of each rung must be operated oppositely. In an inverter, there are eight possible on-off states. In this case, when the upper switch is closing the state of a rung is “1”, and when the lower switch is closing the condition of the rung is “0” [4].

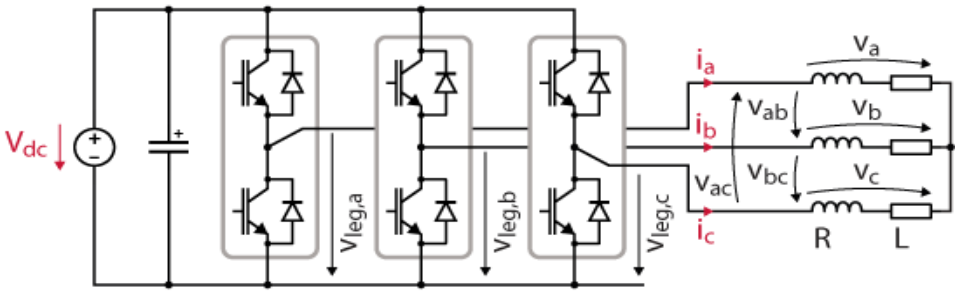

Figure 5. Topology of a two-level inverter with an RL load

Table 1 shows eight space vectors which are summarized in: V0 and V7 are called the zero space vectors because of any phase voltages that are not produced. By contrast, V1 to V6 are known as active space vectors because they generate non-zero phase voltages.

Table 1. Switching States of Inverter with Corresponding Phase Voltages

Space Vector	Leg A state	*Leg B state*	*Leg C state*	V_a	V_b	V_c
V_0	0	0	0	0	0	0
V_1	1	0	0	$2V_{dc}/3$	$-V_{dc}/3$	$-V_{dc}/3$
V_2	1	1	0	$V_{dc}/3$	$V_{dc}/3$	$-2\ V_{dc}/3$
V_3	0	1	0	$V_{dc}/3$	$2\ V_{dc}/3$	$-\ V_{dc}/3$
V_4	0	1	1	$-2\ V_{dc}/3$	$V_{dc}/3$	$V_{dc}/3$
V_5	0	0	1	$-\ V_{dc}/3$	$-\ V_{dc}/3$	$2\ V_{dc}/3$
V_6	1	0	1	$V_{dc}/3$	$-2\ V_{dc}/3$	$V_{dc}/3$
V_7	0	0	0	0	0	0

D. Test Route

The test route is situated at Ayetharyar Town, Southen Shan State, Myanmar as shown in Figure 6. The road has uphill and downhill parts. The required data was collected by driving an ICE car and MATLAB Mobile application.

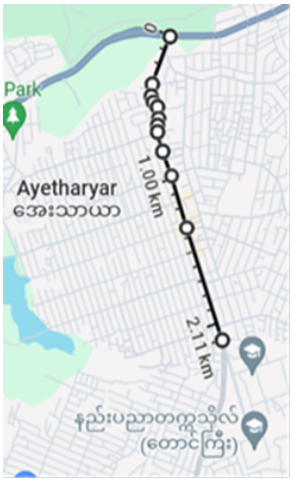

Figure 6. Test Route

The test route altitude over a driving time of 60 sec during test conditions is shown in Figure 8. In this route, the starting point sea level is 989 meters and gradually increases to the highest level of 992 meters and decreases steeply to a lower level of 973 meters. And then the altitude level is increased to the level of 982 meters and there is a little fluctuation.

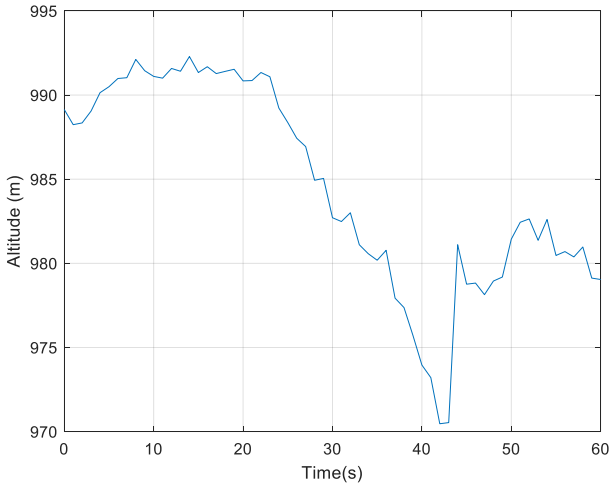

Figure 7. Altitude Changes over Time During Test Conditions

E. Result and Discussion

The decoupling control of the PMSM base drive Nissan Leaf electric vehicle is simulated with two PWM methods. In these closed-loop feedback control methods, the reference speed is obtained by driving an internal combustion engine car in the mountain region of Southen Shan State, Myanmar. This analytical parison is carried out in terms of the energy usage of EVs and the driving range of EVs during

a driving time of 60 sec with five passengers. The parameters used in this simulation study are listed in Tables 2 and 3.

Table 2. Parameters of PMSM

No	Identity	*Value*
1	No. of motor	1
2	Motor type	PMSM
3	Efficiency	95
4	Maximum speed	10000 rpm
5	Rated speed	3000 rpm
6	Max torque	254 Nm
7	Rated power	80 kW

Table 3. Parameters of Electric Vehicle

No	Identity	*Symbol*	*Value*
1	Kerb weight		1450 kg
2	Passenger Weight	One person	70 kg
3	Coefficient of rolling resistance	μ	0.015
4	Air density	ρ	1.2 kg/m^3
5	Width		1.77 m
6	Height		1.549 m
7	Front area	A	2.9141 m^2
8	Drag coefficient	C_d	0.28
9	Gear ratio		7.9377:1
10	Rated Power	P	80 kW
11	Seating Capacity		5
12	Drive System	Front-wheel Drive	
13	Tire radius	R	0.316 m
14	Battery Type	Lithium-ion	
15	Nominal battery pack voltage	V	360 V

The longitudinal motion of the body of a two-axle vehicle is shown in Figure 8. In this Simulink model, body mass, road inclination, aerodynamic drag, and the weight distribution between axles owing to road profile and acceleration are all evaluated.

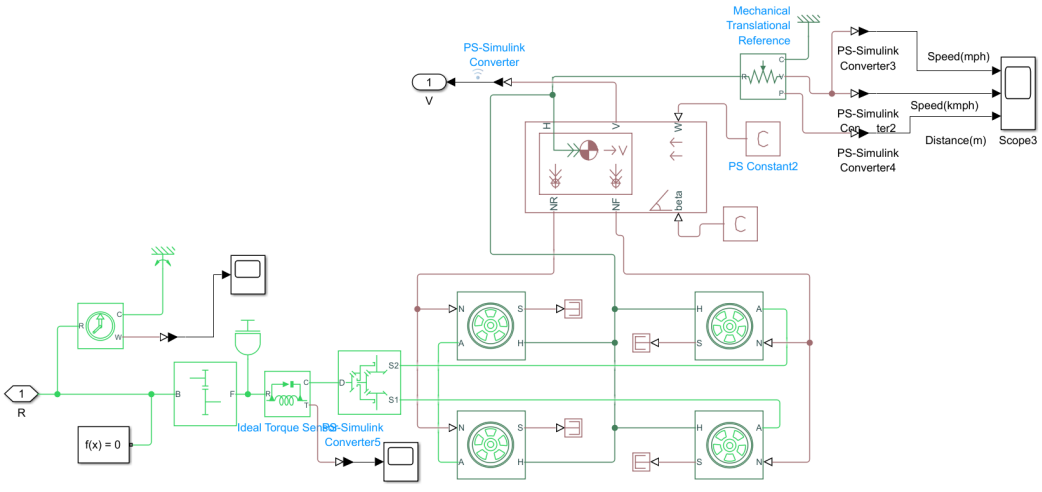

Figure 8. Simulink Model of Vehicle Body

The Simulink models of 80 kW Nissan Leaf EV with SPWM drive PMSM are shown in Figure 9. The Nissan Leaf EV has a battery pack that is located under the floor and between the wheels, which optimizes the vehicle's interior space and handling. This car is a Battery Electric Vehicle (BEV), which is powered only by electricity, and the crab weight of this EV is 1450 Kg. The total weight of a vehicle with five passengers is

Total Mass = Vehicle Kerb weight + passengers weight + Any play load

= 1450 kg +5×70 kg+ 50 kg = 1850 kg

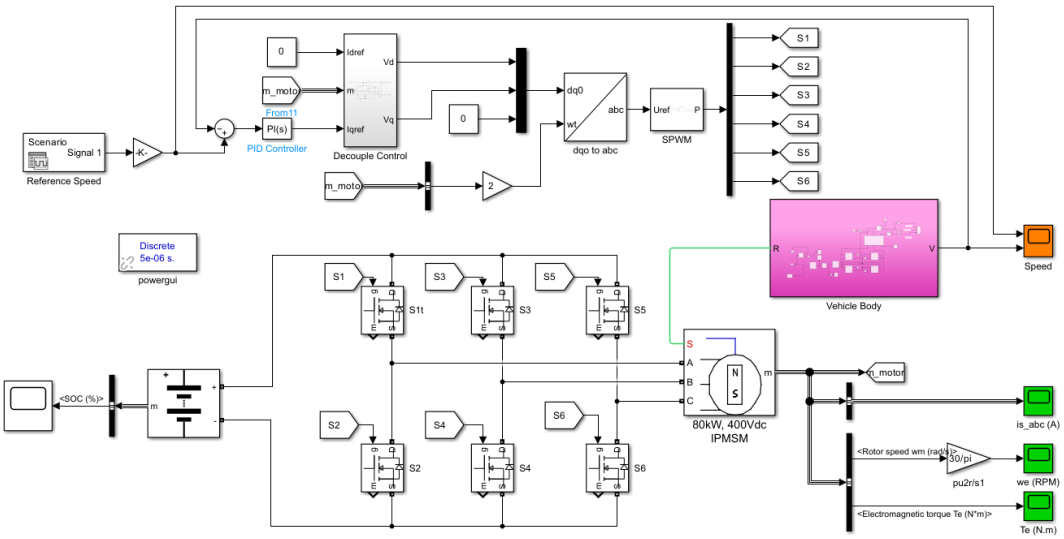

Figure 9. Simulink Model of SPWM Inverter Drive Electric Vehicle

The Simulink models of 80 kW Nissan Leaf EV with SVPWM inverter drive PMSM are shown in Figure 10.

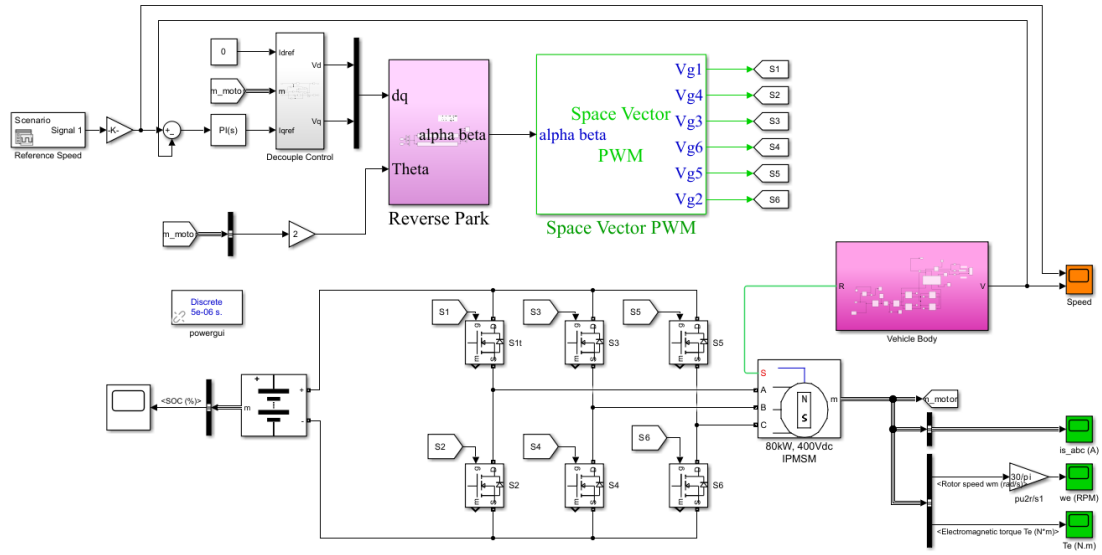

Figure 10. Simulink Model of SVPWM Inverter Drive Electric Vehicle

Figure 11 shows the stator current of PMSM with (a) the SPWM, and (b) SVPWM. During acceleration and deceleration conditions, the motor draws more currents. The maximum current of the SPWM drive motor is 1200 A, and that of the SVPWM drive motor is 600 A during the driving time of 60 sec. In the SPWM Drive, the regular driven current of the motor is lower than the SVPWM drive, but in acceleration conditions, the current drawn from the SPWM drive motor is higher than the SVPWM drive motor.

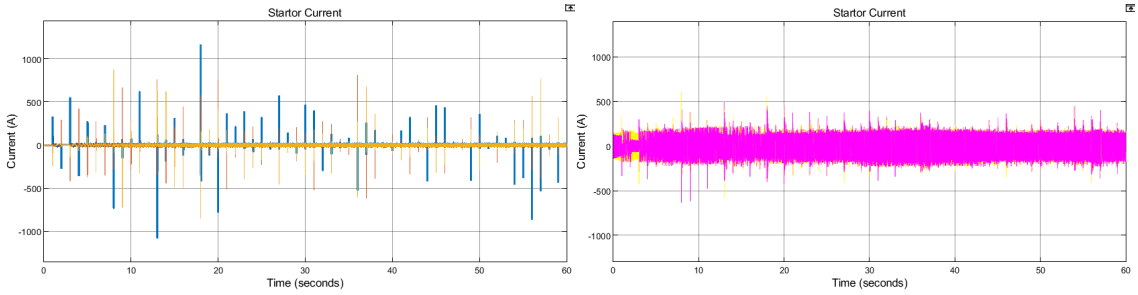

(a) (b)

Figure 11. Stator Currents of PMSM with (a) SPWM, (b) SVPWM

Figure 12 shows the stator current of PMSM with (a) SPWM, and (b) SVPWM. An electric motor with low maximum torque cannot provide high acceleration. The vehicle torque varies with changing acceleration and deceleration during a drive time of 60 sec. In SPWM Drive, the maximum torque is 300 Nm, and in the SVPWM drive, the maximum torque is 280 rpm during the driving time of 60 sec. In normal driven conditions, the torque response of the SPWM drive motor is lower than the SVPWM drive motor. In acceleration conditions, the torque response of the SPWM drive motor is higher than the SVPWM drive motor.

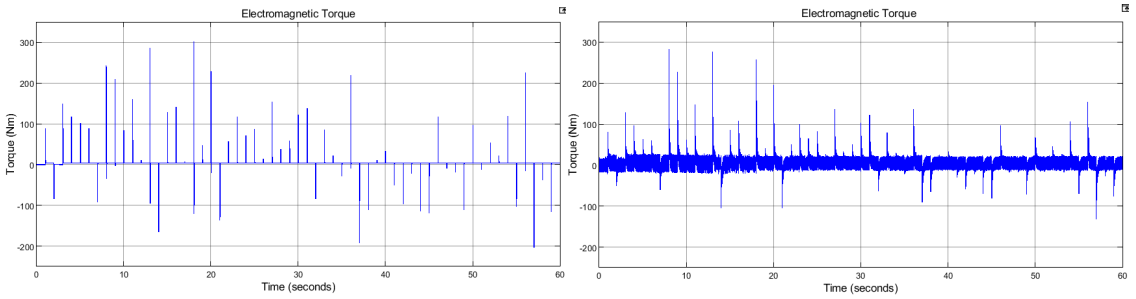

(a) (b)

Figure 12. Torque Response of PMSM with (a) SPWM, (b) SVPWM

Figure.13. shows reference-driven speed and the actual speed of the EV with (a) SPWM, and (b) SVPWM. In SPWM Drive, reference speed and vehicle are identical but overshoot when suddenly change in speed, and in SVPWM Drive, reference speed and vehicle are identical during the driving time of 60 sec.

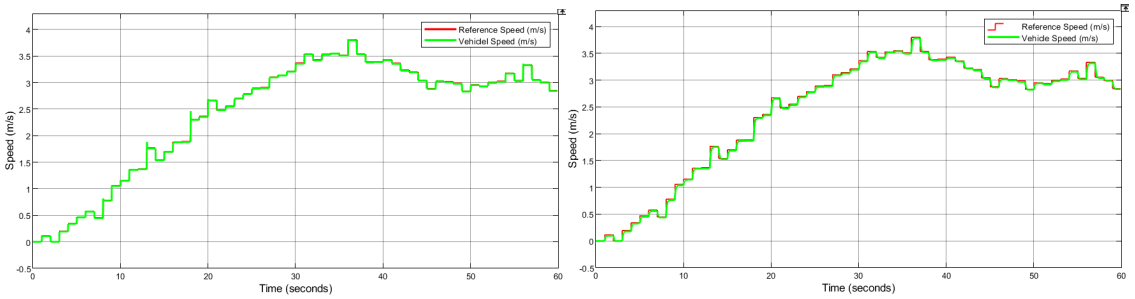

(a) (b)

Figure 13. Reference Speed and Actual Speed of EV with (a) SPWM, (b) SVPWM

Figure 14 shows reference-driven speed and the actual speed of the EV with (a) SPWM, and (b) SVPWM. In SPWM Drive, reference speed and vehicle speed are identical, but overshoot occurs when the speed is suddenly changed, and in SVPWM Drive, reference speed and vehicle speed are identical during the driving time of 60 sec. In the SPWM drive, the speed of PMSM is lower than the speed of the SVPWM drive motor. The maximum speed of the SVPWM drive motor is 2800 rpm, and the maximum speed of the SPWM drive motor is 750 rpm.

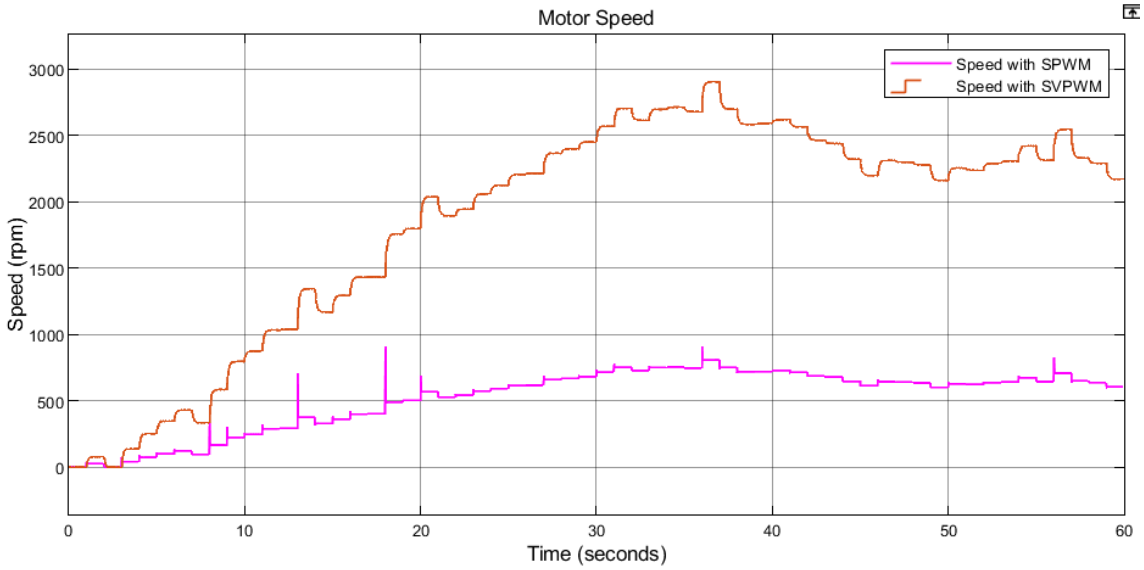

Figure 14. Speed Response of PMSM with (a) SPWM, (b) SVPWM

In this test, the beginning SOC is 60%, and the driving time is 60 sec. The SPWM/SVPWM drive inverter is also applied to compare these drives. The simulation results are shown in Figure 15. In SPWM Drive, SOC the battery depletes to 59.976% from the initial 60%(i.e., consumption of 0.024%), and in SPWM Drive, the SOC of battery depletes to 59.9% from the initial 60%(i.e., consumption of 0.1%). With the SVPWM Drive, the usage of battery SOC is higher than the SPWM Drive.

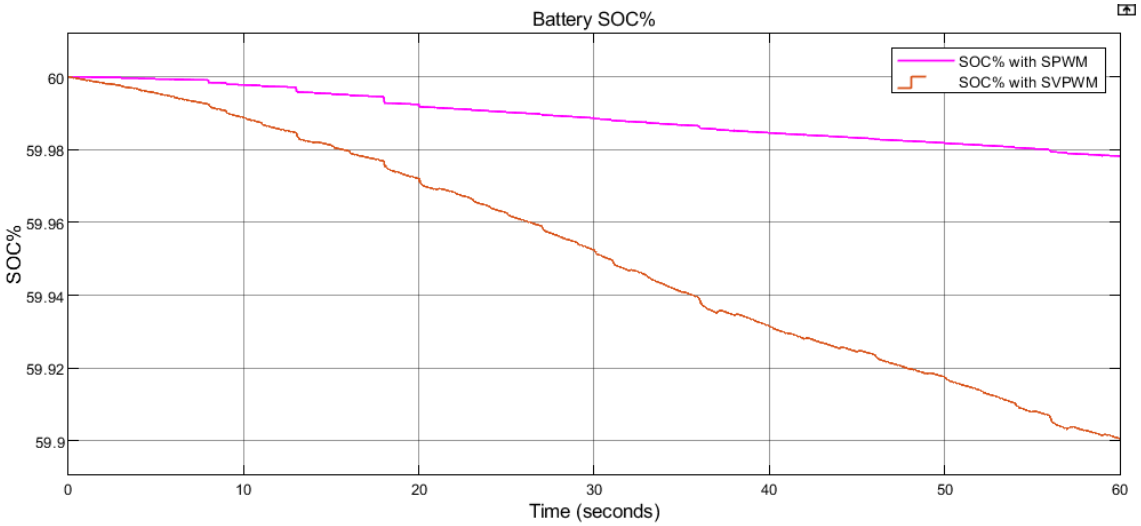

Figure 15. SOC of Battery with (a) SPWM, (b) SVPWM

Figure 16 shows the speed response of EVs with (a) SPWM, and (b) SVPWM. In SPWM Drive, the maximum speed of the electric vehicle is 3.5 km/h, and the overshoot occurs when the speed is suddenly changed. In the SVPWM drive, the maximum speed is 10.3 km/h, and there is no overshoot.

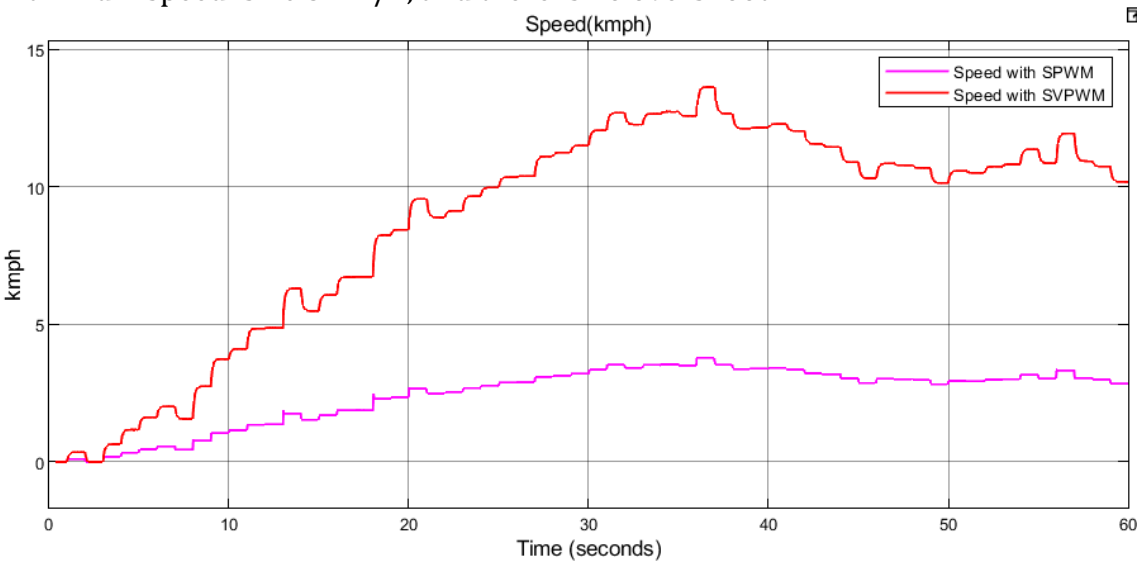

Figure 16. Speed of EV for driving time 60 sec with (a) SPWM, (b) SVPWM

As shown in Figure 17, in SPWM Drive, the vehicle travels 41 m, and with SVPWM Drive, this vehicle travels 141 m in 60 sec. During a driving time of 60 seconds, an SPWM-driven EV is more traveled than an SVPWM-driven EV.

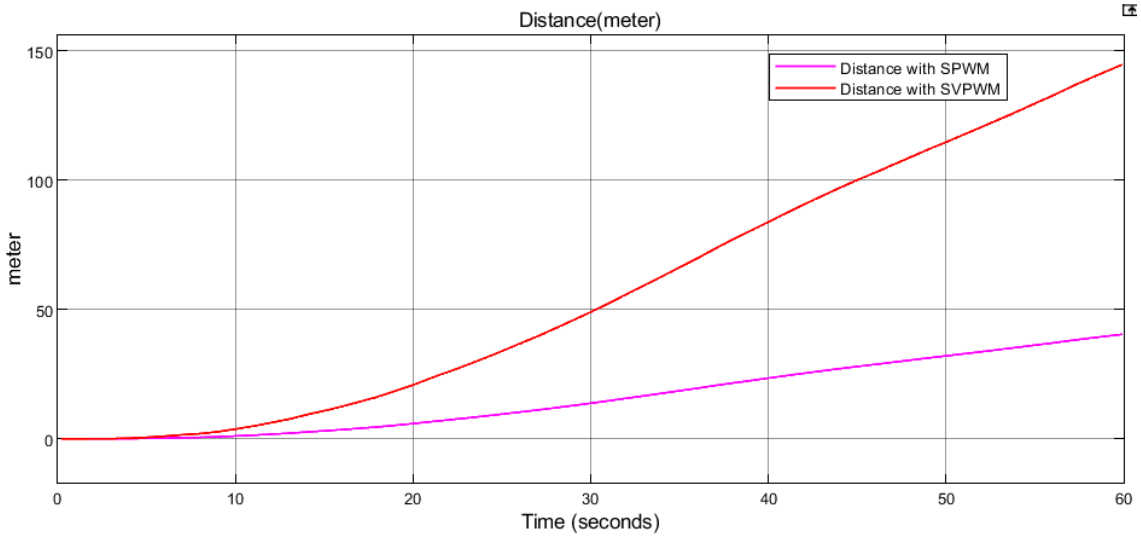

Figure 17. Distance of EV for driving time 60 sec with (a) SPWM, (b) SVPWM

F. Conclusion

This paper analyzes the performance of decoupling control electric vehicles using SPWM and SVPWM. The energy consumption values and the range of an electric vehicle are analyzed by driving SPWM and SVPWM drives. First, by driving an internal combustion engine car in Ayetharyar Town, Southen Shan State, Myanmar, the reference speed of EVs is obtained, and the Simulink model with the parameters of Nissan Leaf four-wheel EV using MATLAB/Simulink. According to the results of tests, in SPWM drive, the vehicle travels 41m in 60 sec, and the SOC of its battery reduces to 59.976% from the initial 60%(i.e., consumption of 0.024%). So, the vehicle consumes 140Wh/km and has a range of 102.5 km, and in SVPWM drive, this vehicle travels 141m in 60 sec, and SOC of the battery reduces to 59.9% from the initial 60%(i.e., consumption of 0.1%). So, the vehicle consumes 160Wh/km and has an 85 km range. By comparison of these results, SPWM drive EV has a higher range and lower energy consumption than SVPWM drive EV. But, in the SVPWM drive, EVs have a good speed response, and overshoots do not occur. In SPWM drive, the speed response is slow, and overshoot occurs when the speed is suddenly changed. In normal driven conditions, the current and torque of the SPWM drive motor are lower than that of the SVPWM drive motor, but in acceleration conditions, the SPWM drive has higher current and torque than the SVPWM drive motor. According to the above discussion, although the SPWM drive has a higher range, SVPWM has a fast speed response and smooth torque response.

G. Acknowledgment

The author would like to express his gratitude to his family and his teachers. The author would like to thank his supervisor for his effective suggestion. The author expresses his thanks to all the people who will be concerned and support the preparation of this paper.

H. References

[1] K. O. Ahmet & S. Hamit, "Modelling of Electric Vehicles with Matlab/Simulink," International Journal of Automotive Science and Technology, Vol. 2, No. 4, 2018.
[2] S. Hitesh & C. Sunanda, "Modeling and Performance Analysis of an Electric Vehicle with MATLAB/Simulink," International Research Journal of Engineering and Technology (IRJET), Volume. 07, Issue. 06, June 2020.
[3] S. Hanlin, L. Xin, L. Guilin & S. Anwen, "A Robust Dynamic Decoupling Control Scheme for PMSM Current Loops Based on Improved Sliding Mode Observer," Journal of Power Electronics, Vol. 18, No. 6, pp. 1708-1719, November 2018.
[4] G. G. Kuheli & G. Amit, "A Comparison on Various PWM Techniques and Performance of Three Phase Induction Motor Based on Those Techniques," International Journal of Science Engineering Technology Research, Vol. 06, Issue. 19, May 2017.
[5] V. Rana, S. Khan, R. S. Ashish, T. Rakholiya & D. Shah, "Modeling, Simulation and Speed Control of PMSM Motor by using MATLAB/Simulink," International Journal of Innovative Research in Science, Engineering, and Technology, Vol. 7, Issue 12, December 2018.
[6] G. Karthikeyan, D. Ruhul, J. M. Shahil. R. R. Kanan & A. Ajmaludeen, "Simulation and Modeling of electric vehicle," International Journal of Advanced Research in Science, munication and Technology (IJARSCT), Vol. 2, Issue. 5, June 2022.
[7] T. Poonam & T. Pawan, "Design & Simulation of Motor Drive for an Electric Vehicle Using MATLAB Simulink," International Journal of Advance Research in Science and Engineering, Vol. 11, Issue. 06, June 2022.
[8] O. K. Ahmet & S. Hamit, "Modelling of an Electric Vehicle with Matlab/Simulink," International Journal of Automotive Science and Technology, Vol. 2, No. 4, November 2018.
[9] S.Hanlin, L.Guilin & S Anwen, "A Robust Dynamic Decoupling Control Scheme for PMSM Current Loops Based on Improved Sliding Mode Observer," Journal of Power Electronics, Vol. 18, pp. 1708-1719, November 2018.